Available online at www.sciencedirect.com
SCIENCE DIRECT®
Journal of Sound and Vibration 294 (2006) 249–268
JOURNAL OF SOUND AND VIBRATION
www.elsevier.com/locate/jsvi

# Nonlinear semi-passive multimodal vibration damping: An efficient probabilistic approach

D. Guyomar, A. Badel*

*Laboratoire de Génie Electrique et Ferroélectricité, INSA de Lyon, 69621 Villeurbanne, France*

Received 11 April 2005; received in revised form 30 September 2005; accepted 7 November 2005
Available online 18 January 2006

**Abstract**

This paper deals with the synchronized switch damping (SSD) technique, a semi-passive approach developed to address the problem of structural vibration damping. This technique takes advantage of an original nonlinear processing of the voltage generated by piezoelements. It was shown that the original control law for the SSD technique was optimal in the case of monomodal excitations. In the case of wide band multimodal excitation it is not true anymore. This paper proposes a novel multimodal control law for the SSD technique. It is based on a probabilistic description of the piezovoltage and results in an optimization of the energy dissipated in the nonlinear device connected to the piezoelectric elements.


## 1. Introduction

The problem of structural vibration damping in many industrial sectors such as automobile, aerospace, sports equipment, measurement devices, etc., has instigated a sharp increase in research in the area of vibration control. In this field, much research has been devoted to piezoelectric vibration control device. Piezoelectric materials are solid state, reliable and of lightweight. They possess relatively high bandwidths and consume relatively small amounts of power. These properties are ideal for operating the materials as sensors, actuators or both sensor and actuator. Piezoelectric materials are embedded or bonded on the vibrating structure. When the structure vibrates, the piezoelectric elements are stressed and convert part of the mechanical energy by piezoelectric effect. Degradation or transfer of this energy results in control and reduction of the vibration. For active vibration control, a complex system built with at least a sensor, a control unit and a feedback actuator is necessary. In addition, external power sources and amplifier are needed for the control unit and the actuators. The passive techniques can be more easily integrated because of their simplicity and their compactness. The piezoelectric elements are connected to a specific electrical network consisting of a dissipative shunt [1]. The most effective method is the tuned shunt where a circuit made with an inductor and a resistor in series is connected to the capacitance of the piezoelements. Optimal damping is obtained by tuning the electrical resonance on the frequency of the structural mode to be damped. This method gives good results but has the following disadvantages: For low-frequency modes, the optimal value of the inductor is very large

*Corresponding author.
*E-mail address:* adrien.badel@insa-lyon.fr (A. Badel).

0022-460X/$ - see front matter © 2005 Elsevier Ltd. All rights reserved.
doi:10.1016/j.jsv.2005.11.010

and requires active circuitry. Moreover, it is sensitive to environmental factors such as temperature and acoustic load, which cause drift in the structure's resonance frequencies. Once detuned, the shunt circuit looses its damping performance. Finally, mutimodal damping requires the use of complex shunt circuits [2].

To bypass these drawbacks, several semi-passive or active–passive techniques have been proposed. In the solid-state tunable piezoelectric absorber developed by Davis and Lesieutre [3], a passive capacitive shunt circuit is used to electrically adjust the piezoelements effective stiffness and then tune the device resonance frequency. In the approach proposed by Morgan and Wang [4], an adaptive inductor tuning, a negative resistance and a coupling enhancement set-up lead to a system with multimodal damping ability.

More recently, switched shunt techniques have been developed introducing a nonlinear approach by changing the piezoelement properties or boundary conditions synchronously with the structure motion. The state-switching method proposed by Clark [5] is a variable stiffness technique in which piezoelements are periodically held in the open-circuit state then switched and held in the short-circuit state, synchronously with the structure motion. Cunefare successfully adapted previous works of Larson et al. [6] on the state-switching concept to vibration damping in a rather different way and proposed the state-switching absorber (SSA) [7].

This paper deals with a particular nonlinear technique which is known as SSD for synchronized switch damping [8–10]. It consists in a nonlinear processing of the voltage on piezoelectric elements bonded on the structure. It is implemented with a simple switch driven during short periods synchronously with the structure motion. The switch connects the piezoelement to a circuit which can be either a simple short circuit (SSDS) or a small inductor (SSDI). It was shown that the original control law governing this technique was optimal for single-frequency excitations [10]. Corr and Clark proposed a multimodal approach which consists in selecting the modes to be controlled and insuring a negative rate of energy change in the selected modes of the structure [11]. They showed at the same time that the original SSD control law was not optimal in the case of wide band multimodal excitation. This paper presents a new control law for the SSD techniques based on the idea of maximizing the energy dissipated in the nonlinear processing device connected to the piezoelectric elements. It is derived from a probabilistic description of the piezovoltage. Since the SSDI technique is more efficient than the SSDS technique, we mainly focused on this technique in the present paper, but the probabilistic approach is also valid for the SSDS.

A multimodal modelling of a clamped–free beam with piezoelectric elements is presented in Section 2. It is based on the model developed by Sodano et al. to address piezoelectric energy harvesting problem [12]. The different control laws are detailed in Section 3. Simulations results are given and discussed in Section 4.

## 2. Modelling

A typical vibrating beam damped by the action of piezoelectric elements is considered, as shown in Fig. 1. The beam is clamped at one end in a rigid structure and piezoelectric inserts are bonded on its surface close to the clamped end where the bending radius is a minimum. In the considered case, the piezoelectric elements are massive ceramics whose poling directions are perpendicular to the beam. It is then the lateral coupling $k_{31}$ which mainly drives the piezoelectric response. This approach can also be generalized to composite piezoelectric inserts where the poling direction may be horizontal. The two piezoelectric elements are electrically connected in parallel. The ground is set to the electrical potential on the piezoelectric elements surfaces in contact with the beam. The characteristics of the beam and of the piezoelectric elements are summarized in Table 1.

It is assumed that the structure acts as pure Euler–Bernoulli beam, the stress $T$ and the strain $S$ in the structure are then essentially longitudinal (along the $x$-axis). The electric field $E$ is purely along the $y$-axis, and

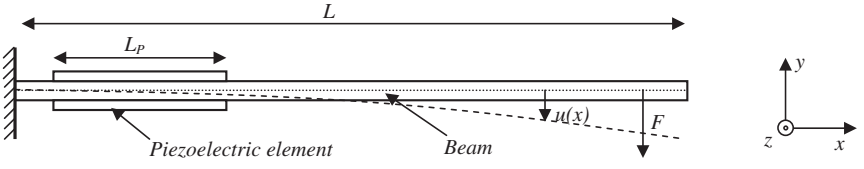


Fig. 1. Vibrating beam with piezoelectric elements.

Table 1
Structure characteristics

| | |
|---|---|
| Structure width | $b$ |
| Beam length | $L$ |
| Beam volume | $V_B$ |
| Beam density | $\rho_B$ |
| Beam stiffness | $c_B$ |
| Piezoelements length | $L_p$ |
| Piezoelements thickness | $e_p$ |
| Piezoelements volume | $V_P$ |
| Piezoelements density | $\rho_P$ |
| Short-circuit piezoelements stiffness | $c_P^E$ |
| Open-circuit piezoelements stiffness | $c_P^D$ |
| Piezoelements clamped permittivity | $\varepsilon^S$ |
| Piezoelectric coefficient | $e$ |

so is the electrical displacement $D$. The piezoelectric constitutive equations are then given by Eq. (1), where $c_P^E$ is the longitudinal elastic stiffness of the piezoelements when they are short circuited, $\varepsilon^S$ is their clamped permittivity and $e$ the piezoelectric coefficient. In the beam, the relationship between stress and strain is given by Eq. (2), where $c_B$ is the longitudinal elastic stiffness of the beam.

$$\begin{bmatrix} T_x \\ D_y \end{bmatrix} = \begin{bmatrix} c_P^E & -e \\ e & \varepsilon^S \end{bmatrix} \begin{bmatrix} S_x \\ E_y \end{bmatrix}, \tag{1}$$

$$T_x = c_B S_x. \tag{2}$$

In order to give a simple multimodal lumped model for the cantilever beam with piezoelectric elements, some assumptions must be made. The first assumption is that the motion time and space variables can be separated. The displacement of the beam can thus be written as the summation of modes in the beam and a temporal coordinate. This is shown in Eq. (3), where $\phi_j(x)$ is the mode shapes of the structure, $r_j(t)$ the corresponding temporal coordinate and $N$ the number of mode included in the analysis. The mode shape determination can be done assuming that the structure is homogeneous along the $x$-axis and using typical analytical mode shape for Euler–Bernoulli beams, or using FEM software. The second assumption is the Euler–Bernoulli one, which allows the strain in the structure to be the product of the distance from the neural axis and the second spatial derivative of the displacement along the beam, which is summarized in Eq. (4). The last assumption is that the electric field along the thickness of the piezoelements is constant and linked to the piezovoltage $V$ by Eq. (5).

$$u(x,t) = \sum_{j=1}^{N} \phi_j(x) r_j(t), \tag{3}$$

$$S_x = -yu''(x,t) = -y \sum_{j=1}^{N} \phi_j''(x) r_j(t), \tag{4}$$

$$\begin{aligned} E_y &= -\frac{V}{e_p} \quad \text{for } y>0, \\ E_y &= \frac{V}{e_p} \quad \text{for } y<0. \end{aligned} \tag{5}$$

It is considered that the structure is driven by a punctual force $F$, at the abscissa $x_F$. Using previous assumptions, it was shown [12] that the constitutive equations of the system, governing the displacement of the structure and its electrical behaviour can be expressed by Eqs. (6) and (7). The different parameters and variable of these equations are detailed in Tables 2 and 3, respectively. The $j$th equivalent damper $C_j$ is

Table 2
Parameters of the model

| | |
|---|---|
| *Main parameters* | |
| $j$th beam dynamic mass | $M_{Bj} = \rho_B \int_{V_B} \phi_j(x)^2 \, \mathrm{d}V_B$ |
| $j$th piezoelements dynamic mass | $M_{Pj} = \rho_P \int_{V_P} \phi_j(x)^2 \, \mathrm{d}V_P$ |
| $j$th beam equivalent stiffness | $K_{Bj} = c_B \int_{V_B} y^2 \phi_j''(x)^2 \, \mathrm{d}V_B$ |
| $j$th short-circuit piezoelements equivalent stiffness | $K_{Pj}^E = c_P^E \int_{V_P} y^2 \phi_j''(x)^2 \, \mathrm{d}V_P$ |
| $j$th macroscopic piezoelectric coefficient | $\alpha_j = e \int_{V_P} \frac{\lvert y \rvert}{e_P} \phi_j''(x) \, \mathrm{d}V_P$ |
| $j$th force coefficient | $\beta_j = \phi_j(x_F)$ |
| Piezoelements clamped capacitance | $C_0 = 2\frac{\varepsilon_S L_P b}{e_P}$ |
| *Derived parameters* | |
| $j$th open-circuit piezoelements equivalent stiffness | $K_{Pj}^D = c_P^D \int_{V_P} y^2 \phi_j''(x)^2 \, \mathrm{d}V_P = K_{Pj}^E + \frac{\alpha_j^2}{C_0}$ |
| $j$th short-circuit resonance frequency | $\omega_j^E = \sqrt{\frac{K_{Sj} + K_{Pj}^E}{M_{Sj} + M_{Pj}}}$ |
| $j$th open-circuit resonance frequency | $\omega_j^D = \sqrt{\frac{K_{Sj} + K_{Pj}^D}{M_{Sj} + M_{Pj}}}$ |
| $j$th squared coupling coefficient | $k_j^2 = \frac{(\omega_j^D)^2 - (\omega_j^E)^2}{(\omega_j^D)^2} = \frac{\alpha_j^2}{(K_{Sj} + K_{Pj}^D)C_0}$ |
| $j$th equivalent damper | $C_j = \frac{\sqrt{(K_{Sj} + K_{Pj}^D)(M_{Sj} + M_{Pj})}}{Q_{mj}}$ |

Table 3
Variables of the model

| | |
|---|---|
| Piezoelements voltage | $V$ |
| Piezoelements outgoing current | $I$ |
| $j$th displacement temporal coordinate | $r_j$ |

deduced from the other parameters of the model and from the mechanical quality factor $Q_{mj}$ associated to the $j$th mode, as shown in Table 2.

$$\forall j = 1 \ldots N \quad (M_{Sj} + M_{Pj})\ddot{r}_j + (K_{Sj} + K_{Pj}^E)r_j + C_j\dot{r}_j - \alpha_j V = \beta_j F, \tag{6}$$

$$I = \sum_{j=1}^{N} \alpha_j \dot{r}_j - C_0 \dot{V}. \tag{7}$$

A cantilever beam with piezoelectric elements can then be modelled by the sum of mechanical oscillators corresponding to each resonance frequency of the structure. The displacement of the dynamic mass of the $j$th oscillator is $r_j$. Without piezoelectric elements, the motion of the different mechanical oscillators would be perfectly independent and unique functions of the driving force. It is the electromechanical properties of the piezoelectric elements which links the motion of the different mechanical oscillators to the voltage. It is here pointed out that a nonlinear processing of the piezovoltage may affect all modes of the structure.

## 3. Control Laws

### 3.1. Energetic analysis

It is considered that an electrical circuit is connected to the piezoelectric elements. This device is designed to have a damping effect on the structure. The global energy equation (8) is the summation of the $N$ energy equations associated to each mode by multiplying both sides of Eq. (6) by the speed and integrating over the time variable. The provided energy $E_P$ is divided into the mechanical energy $E_M$ (kinetic + elastic), the viscous losses $E_V$, and the transferred energy $E_S$ which corresponds to the part of mechanical energy which is converted into electrical energy. These energies are summarized in Table 4.

Multiplying both terms of Eq. (7) by the voltage and integrating over the time variable shows that the transferred energy is the sum of the electrostatic energy stored on the piezoelectric elements and the energy absorbed by the connected electrical device. The electrical output power can then be considered as losses when the time integral of $VI$ is positive. In the case of vibration damping, the electrical device connected to the piezoelectric elements is then designed to maximize its own consumption. A new energetic equation (9) can then be given, expressing the provided energy as the sum of the kinetic energy $E_{\text{kin}}$, the potential energy $E_{\text{pot}}$ (electrostatic + elastic) and the dissipated energy $E_D$ (viscous losses + energy consumed in the electrical device). These energies are detailed in Table 5.

$$E_P = E_M + E_V + E_S, \tag{8}$$

$$E_P = E_{\text{pot}} + E_{\text{kin}} + E_D. \tag{9}$$

### 3.2. SSDI basics

This paper deals with a particular nonlinear technique which is known as SSDI for Synchronized Switch Damping on Inductor [8–10]. This nonlinear damping technique consists of adding a switching device in parallel with the piezoelectric elements. It allows to briefly inverse the piezovoltage at selected instants. This device is composed of a switch and an inductance $L_I$ connected in series. The switch is almost always open. It

Table 4
Energetic terms #1

| | |
|---|---|
| Provided energy | $E_F = \sum_{j=1}^{N} \beta_j \int_0^t F\dot{r}_j \, \mathrm{d}t$ |
| Mechanical energy | $E_M = \frac{1}{2}\sum_{j=1}^{N}(M_{Sj} + M_{Pj})\dot{r}_j^2 + \frac{1}{2}\sum_{j=1}^{N}(K_{Sj} + K_{Pj}^E)r_j^2$ |
| Viscous losses | $E_V = \sum_{j=1}^{N} C_j \int_0^t \dot{r}_j^2 \, \mathrm{d}t$ |
| Extracted energy | $E_S = \sum_{j=1}^{N} \alpha_j \int_0^t \dot{r}_j V \, \mathrm{d}t = \frac{1}{2} C_0 V^2 + \int_0^t VI \, \mathrm{d}t$ |

Table 5
Energetic terms #2

| | |
|---|---|
| Kinetic energy | $E_{\text{kin}} = \frac{1}{2}\sum_{j=1}^{N}(M_{Sj} + M_{Pj})\dot{r}_j^2$ |
| Potential energy | $E_{\text{pot}} = \frac{1}{2}\sum_{j=1}^{N}(K_{Sj} + K_{Pj}^E)r_j^2 + \frac{1}{2}C_0 V^2$ |
| Dissipated energy | $E_D = \sum_{j=1}^{N} C_j \int_0^t \dot{r}_j^2 \, \mathrm{d}t + \int_0^t VI \, \mathrm{d}t$ |

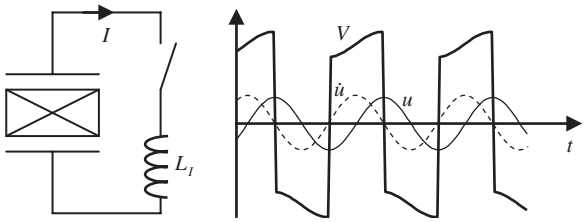


Fig. 2. SSDI device and voltage and displacement typical waveforms for a sinusoidal excitation.

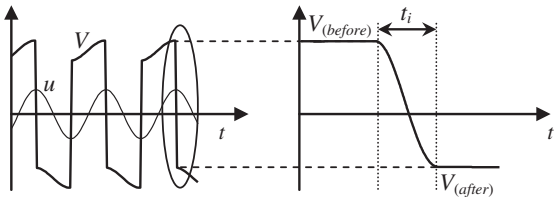


Fig. 3. Piezoelement voltage inversion.

is briefly closed at selected instants. The capacitance $C_0$ of the piezoelectric elements and the inductance $L_I$ constitute then an oscillator. The switch is kept closed until the voltage $V$ on the piezoelectric elements has been inversed. It corresponds to a time $t_i$ equal to a semi-pseudo-period of the electric oscillator, as shown in Eq. (10). The lower the inductance $L_I$, the shorter will be $t_i$. Thus, this technique does not require a high inductance value. Practically, the inductance is chosen to get an inversion time roughly between 20 and 50 times lower than the shortest mechanical vibration period.

$$t_i = \pi\sqrt{L_I C_0}. \tag{10}$$

When the switch is open and if no load is connected, the outgoing piezocurrent is null and then the voltage and the displacement vary proportionally. The voltage and displacement typical waveforms are shown in Fig. 2 in the case of a sinusoidal excitation and when the voltage inversion instants correspond to the displacement extrema. The voltage inversion is detailed in Fig. 3.

The voltage inversion is not perfect, because a part of the energy stored on the piezoelectric elements capacitance is lost in the switching network (electronic switch + inductance). These losses are modelled by an electrical quality factor $Q_I$. The relation between $Q_I$ and the voltage of the piezoelectric element before and after the inversion process is given by Eq. (11). Because of this nonlinear process, a voltage magnification is obtained and a phase shift appears between the displacement and the voltage which result in optimizing the extracted energy. It was shown [8] that processing the voltage on each of its extrema was optimal in the case of

sinusoidal single-frequency excitations. As shown in Fig. 2, the piezovoltage can be expressed by the sum of a sinusoidal function and of a crenel function. When switching on each extremum, the crenel voltage generates a mechanical force that is always opposite to the sign of the speed, resulting in a drastic damping effect. Since the created force is proportional to the sign of the speed, it means that the dissipative mechanism is of the dry friction type. A dry friction mechanism dissipates an energy which is unlike the viscous mechanism independent of the frequency. The proposed approach works thus also on very low frequency.

In the case of the SSDS technique, the voltage is not inversed but simply cancelled. The SSDS technique corresponds then to the case where $\gamma = 0$.

$$V_{(\text{after})} = -\gamma V_{(\text{before})} = -V_{(\text{before})}\, \mathrm{e}^{-\pi/2Q_I}. \tag{11}$$

### 3.3. Multimodal law by modes selection

In the case of multimodal excitations, the switching law consisting in inversing the voltage at each strain extremum in the piezoelements is no more optimal. A smart multimodal law was proposed by Corr and Clark [10] based on the idea of insuring a positive extracted power for selected controlled mode. The global extracted power is derived from the global extracted energy and is given by Eq. (12). If $M$ is the set of modes to be controlled, the extracted power for the selected modes $P_{\text{SM}}$ is given by Eq. (13). The technique proposed by Corr and Clark [10] consists in inversing the voltage at each time that the sign of $\sum_{j\in M} \alpha_j \dot{r}_j$ change, so that $P_{\text{SM}}$ remains always positive.

$$P_S = \sum_{j=1}^{N} \alpha_j \dot{r}_j V, \tag{12}$$

$$P_{\text{SM}} = \sum_{j\in M} \alpha_j \dot{r}_j V. \tag{13}$$

It can be noted that when the piezoelectric elements are open-circuited, the voltage $V$ vary proportionally to $\sum_{j=1}^{N} \alpha_j r_j$, as it can be derived from Eq. (7). Actually $\sum_{j=1}^{N} \alpha_j r_j$ is proportional to the strain in the piezoelectric elements. If all $N$ modes are controlled, this method then consists in processing the piezovoltage at each strain extremum, which corresponds to the earlier control law proposed for the SSD technique. It can also be noted that this technique requires refined filtering devices in order to select modes to be controlled. Filtering inevitably leads to time shifts that result in a lack of effectiveness.

### 3.4. Multimodal probabilistic-based control law

The approach proposed in this paper consists in optimizing the energy dissipated in the switching device without taking into account any information related to the different modes of the structure.

The consumption of the switching device is always zero except during the voltage inversion when it is equal to the difference of the electrostatic energy on the piezoelectric elements on the voltage inversion jump. The energy dissipated in the switching device is then given by Eq. (14), where $V_k$ is the piezovoltage just before the $k$th inversion. It appears then that maximizing the consumption of the switching device corresponds to maximizing the sum of the squared piezovoltage before each inversion. In other words, optimizing the damping corresponds to finding the switch sequence that maximizes Eq. (14).

$$\int_0^t VI \,\mathrm{d}t = \frac{1}{2} C_0 \sum_k V_k^2 (1-\gamma^2). \tag{14}$$

The probabilistic approach is based on the idea of letting the voltage reach a significant but statistically probable value $v_{\min}$ before processing the voltage inversion. Since the time derivative of the extracted energy cancels when the time derivative of the strain in the piezoelectric element vanishes, the extracted energy reaches a local extremum at each extremum of the strain in the piezoelements. Since strain and voltage

extrema occurs at the same time, the piezovoltage inversion is achieved when $V^2 > v_{\min}^2$ and $V^2$ reaches an extremum.

The piezovoltage is a piecewise continuous function. Its evolution between two inversion processes is given by Eq. (15), where $t_k$ and $t_{k+1}$ are two consecutive switching times, $-\gamma V_k$ is the voltage after the first voltage inversion and $r_{jk}$ is the $j$th temporal coordinate of the displacement at instant $t_k$:

$$\text{for } t \in ]t_k, t_{k+1}] \quad V(t) = -\gamma V_k + \frac{1}{C_0}\sum_{j=1}^{N} \alpha_j (r_j(t) - r_{jk}). \tag{15}$$

After the $k$th inversion time, $V$ can be considered as a continuous function, whose cumulative distribution function is defined by Eq. (16). $v_{\min}$ is defined after each voltage inversion so that the probability of observing $V^2 > v_{\min}^2$ is equal to $P_{SW}$, where $P_{SW}$ is a fixed probability set by the user. This is summarized in Eq. (17), where it is pointed out that $v_{\min}$ can be determined using the cumulative distribution function. Fig. 4 gives a graphical representation of Eq. (17).

$$F_{V^2}(v^2) = P[V^2 \leqslant v^2], \tag{16}$$

$$P[V^2 > v_{\min}^2] = P_{SW} = 1 - F_{V^2}(v_{\min}^2). \tag{17}$$

The critical point of this approach consists in estimating the cumulative distribution function of the voltage after each inversion. It is then easy to determine $v_{\min}$. The evolution of the piezovoltage after the $k$th inversion time can be estimated using Eq. (18) where it is assumed that the strain cumulative distribution function is a slow varying function over the estimation time interval. The strain in the piezoelectric elements after the switch is thus assumed to be similar to the strain in the piezoelectric elements before the switch. The estimation is made using an observation time $T_{es}$ of the strain. The value of $T_{es}$ is set by the user. Its typical value is about two times the period corresponding to the lower resonance frequency. This procedure is illustrated in Fig. 5.

$$V_{es}(t^+) = -\gamma V_k + \frac{1}{C_0}\sum_{j=1}^{N} \alpha_j (r_j(t^-) - r_{jk}) \quad \text{with} \begin{cases} t^+ \in [t_k, t_k + T_{es}] \text{ (future)}, \\ t^- \in [t_k - T_{es}, t_k] \text{ (past)}. \end{cases} \tag{18}$$

It is then assumed that the cumulative distribution function of the piezovoltage after the $k$th inversion time is almost equal to the one of the estimated piezovoltage. This function can be derived from the estimated piezovoltage as shown by Eq. (19) where $t_{V_{es}^2 \leqslant v_{es}^2}$ is the cumulative time where $V_{es}^2 \leqslant v_{es}^2$.

$$F_{V^2}(v^2) \approx F_{V_{es}^2}(v_{es}^2) = P[V_{es}^2 \leqslant v_{es}^2] = \frac{t_{V_{es}^2 \leqslant v_{es}^2}}{T_{es}}. \tag{19}$$

Practically, the estimation of the piezovoltage can be made using an open-circuited additional piezoelement bonded in the same area than the piezoelements used for the vibration control. This piezoelement is used as a strain sensor. Its voltage $V_s$ is given by Eq. (20). Using a $T_{es}$ recording of this voltage before the $k$th inversion, the estimated piezovoltage can be estimated using Eq. (21) where $V_{Sk}$ is the voltage on the sensor at the instant

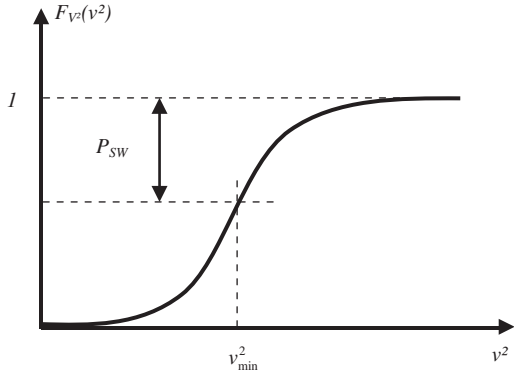


Fig. 4. Determination of $v_{\min}$.

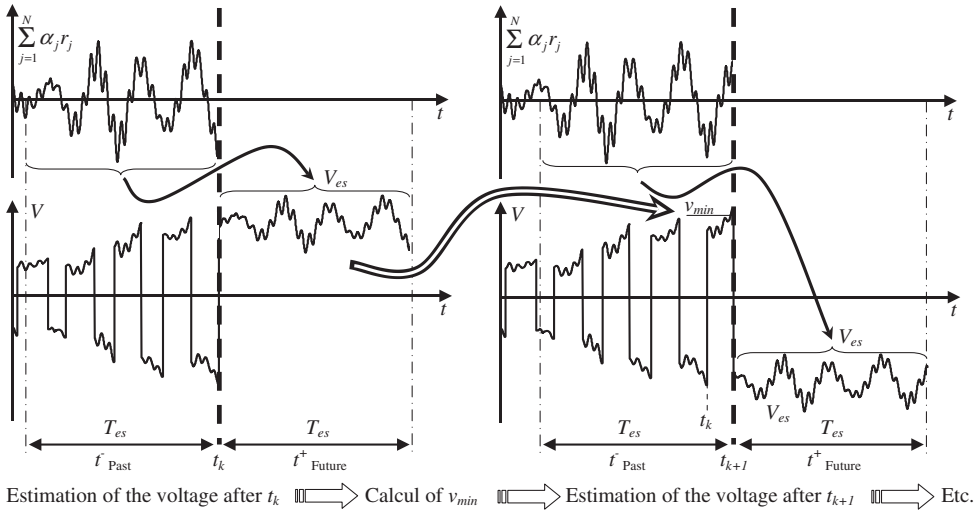


Fig. 5. Estimation of the piezovoltage after an inversion process.

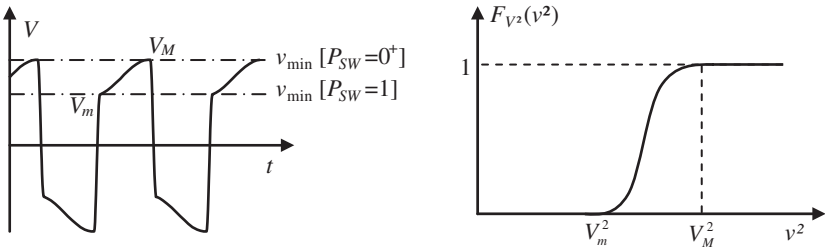


Fig. 6. Probabilistic approach in the case of a monomodal excitation.

$t_k$. It is clear that Eq. (21) is strictly equivalent to Eq. (18), thus this technique can be easily implemented and does not require any filtering device.

$$V_s = \frac{1}{C_0} \sum_{j=1}^{N} \alpha_j r_j, \tag{20}$$

$$V_{\text{es}}(t^+) = -\gamma V_k + V_S(t^-) - V_{Sk}. \tag{21}$$

### 3.5. *Single frequency: a particular case of the probabilistic approach*

In the case of a monomodal excitation and provided that $P_{\text{SW}} > 0$, the probabilistic approach basically leads to inverse the voltage at each displacement extremum, i.e. at each voltage extremum. This is illustrated in Fig. 6. The former SSDI control law developed on single frequency signals, which consists in inversing the voltage on each voltage extremum [8–10], appears then to be a particular case of the probabilistic approach.

## 4. Simulations results

In this section, the probabilistic approach is applied on a three modes model of a cantilever beam with piezoelectric patches and compared to the multimodal law by mode selection. Simulations are derived from numerical time domain integrations of Eqs. (6) and (7). Calculations are made using a fourth-order Runge–Kutta algorithm with a constant integration time step.

### 4.1. Characteristics of the model used for simulations

The model corresponds to a steel beam with piezoelectric elements bonded on its surface driven by a force applied at its free end. Piezoelectric patches are modelled using P189 PZT (NAVY III type) ceramics characteristics. This model roughly corresponds to a real experimental set-up, but the probabilistic approach has not been experimentally tested yet. The first three bending modes are considered. The main characteristics of this structure are summarized in Table 6. The first three resonance frequencies as well as the corresponding coupling coefficients and mode shapes (plotted in Fig. 7) were determined using a FEM simulation of the structure. The parameters of the model can be deduced from these characteristics. They are detailed in Table 7.

### 4.2. Evaluation of the vibration control effectiveness

The effectiveness of the different vibration control laws will be evaluated using two criteria. The first one is related to the displacement of the structure. It is considered the integral $I_u$ of the squared displacement along the $x$-axis and over the time. This double integral is equal to the sum of the integral over the time of the squared displacement temporal coordinate $r_j$, as shown in Eq. (22). The ratio of this double integral in the controlled case and in the uncontrolled case is defined as the 'displacement damping' $A_u$, defined by Eq. (23). The displacement damping in dB is given by Eq. (24).

$$I_u = \int_0^t \int_0^L u(x,t)^2 \,\mathrm{d}x \,\mathrm{d}t = \sum_{j=1}^{N} \int_0^t r_j(t)^2 \,\mathrm{d}t, \tag{22}$$

Table 6
Characteristics of the structure

| | |
|---|---|
| Beam material | Steel |
| Beam dimension | $180 \times 90 \times 2\,\mathrm{mm}^3$ |
| Piezoelements material | P189 (Navy III type) |
| Number of piezoelements | 2 |
| Piezoelement dimension | $40 \times 90 \times 0.3\,\mathrm{mm}^3$ |
| Piezoelements position | 5 mm from clamped end |
| Piezoelements clamped capacitance $C_0$ | 74.9 nF |
| Inversion quality factor $Q_I$ | 5 |
| Resonance frequencies | 56.4 Hz, 353 Hz, 990 Hz |
| Squared coupling coefficients | 0.0092, 0.0044, 0.0007 |
| Mechanical quality factors | 400, 400, 400 |

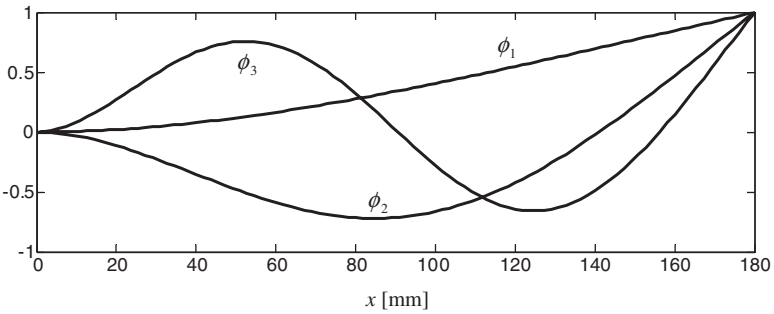


Fig. 7. Mode shapes of the structure.

Table 7
Parameters of the model

| | First mode | Second mode | Third mode |
|---|---|---|---|
| $M_{Sj} + M_{Pj}$ (g) | 62.0 | 62.0 | 62.0 |
| $K_{Sj} + K_{Pj}^{E}$ (N m$^{-1}$) | 7710 | 30 500 | 2 400 000 |
| $C_j$ (N m$^{-1}$ s$^{-1}$) | 0.0549 | 0.344 | 0.964 |
| $\alpha_j$ (N V$^{-1}$) | 0.00230 | 0.0100 | 0.0111 |
| $\beta_j$ | 1 | 1 | 1 |

$$A_u = \frac{(I_u)_{\text{controlled}}}{(I_u)_{\text{uncontrolled}}}, \tag{23}$$

$$A_{u\text{dB}} = 10\ \log(A_u). \tag{24}$$

The second criterion is based on the mechanical energy of the structure. The integral $I_E$ of the structure mechanical energy over the time is given by Eq. (25). The 'energy damping' is defined as the ratio of this integral in the controlled case and in the uncontrolled case, as shown by Eq. (26). Its expression in dB is given by Eq. (27).

$$I_E = \frac{1}{2}\sum_{j=1}^{N}\left[(M_{Sj} + M_{Pj})\int_0^t \dot{r}_j^2\ \mathrm{d}t + (K_{Sj} + K_{Pj}^{E})\int_0^t r_j^2\ \mathrm{d}t\right], \tag{25}$$

$$A_E = \frac{(I_E)_{\text{controlled}}}{(I_E)_{\text{uncontrolled}}}, \tag{26}$$

$$A_{E\text{dB}} = 10\ \log(A_E). \tag{27}$$

### 4.3. Simulations for a pulsed excitation

In this section, a pulsed excitation is applied at the free end of the beam. Simulations are achieved using both the probabilistic law and the multimodal law by modes selection. Calculations are performed for 20 periods of the first resonance frequency. The fixed integration time step is chosen so that there are 50 time steps per period of the higher (the third) resonance frequency. In the case of the probabilistic law, simulations are performed using a strain observation time $T_{\text{es}}$ equal to twice the period corresponding to the lower resonance frequency of the structure. This time must be large enough to get a realistic image of the strain but must also be short enough to allow the technique to be sufficiently reactive. It appears that twice the period of the lower resonance frequency is the best compromise, but taking $T_{\text{es}}$ anywhere between one and three times this period gives satisfactory results.

Fig. 8 shows the displacement and energy damping in dB using the probabilistic control law as a function of $P_{\text{SW}}$. When $P_{\text{SW}}$ is zero, both dampings are zero because $v_{\min}$ is chosen so that the probability of observing $V$ higher than $v_{\min}$ is zero. $P_{\text{SW}} = 0$ corresponds then to the uncontrolled case. When $P_{\text{SW}} = 1$ $v_{\min}$ is chosen so that the probability of observing $V$ higher than $v_{\min}$ is one which results in processing the voltage on each strain extrema. It is shown that for an optimal value of $P_{\text{SW}}$ equal to 0.1 the displacement and energy damping are optimized. The displacement damping reaches $-7.7$ dB and the energy damping $-6.5$ dB whereas it is $-3.8$ and $-4.8$ dB, respectively, when inversing the voltage on each strain extrema.

Fig. 9 shows a comparison between energy and displacement damping using both modes selection control law and probabilistic law. Each possibilities of modes selection are considered. The subtitle 000 corresponds to no mode controlled, 100 only first mode controlled, 111 all modes controlled, etc. The first plot shows the energy damping. A bar is plotted for each considered control law. Each bar is composed of three patches. The bottom patch represents the mechanical energy related to the first mode, the middle patch to the second mode and the top patch to the third mode. It is shown that the best damping with the modes selection law is

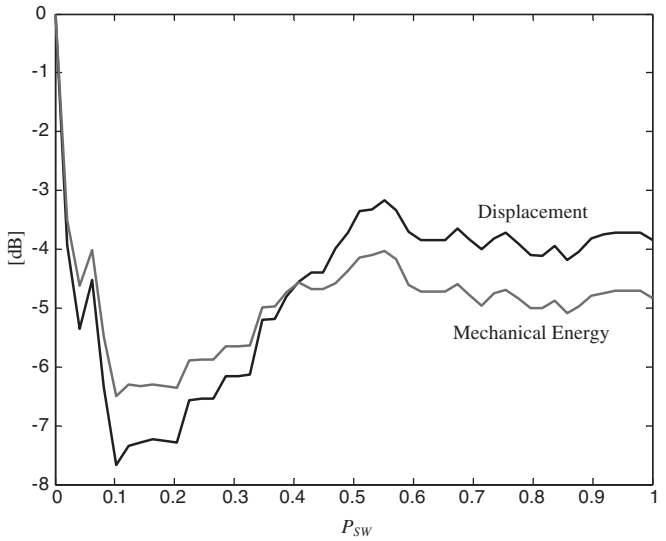


Fig. 8. Pulsed excitation—displacement and energy damping with the probabilistic law as a function of $P_{\mathrm{SW}}$.

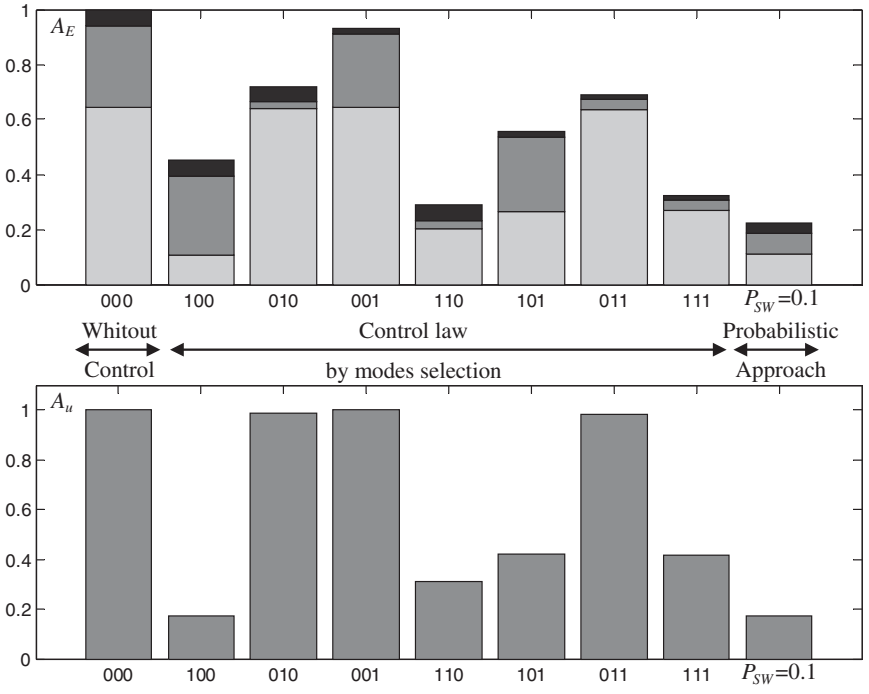


Fig. 9. Pulsed excitation—energy and displacement damping with both modes-selection law and probabilistic law.

obtained when controlling both first and second modes. It reaches $-5.4$ dB whereas it is $-6.5$ dB using the probabilistic approach with $P_{\mathrm{SW}} = 0.1$. The second plot corresponds the displacement damping. It is shown that controlling only the first mode gives the best displacement damping using the modes selection law. It reaches $-7.6$ dB compared to $-7.7$ dB using the probabilistic approach.

Simulations show that both energy and displacement damping benefits from the probabilistic approach. Moreover, this approach allows to optimize both energy and displacement criteria simultaneously, whereas the controlled modes for optimal displacement and optimal energy damping are not the same using the modes

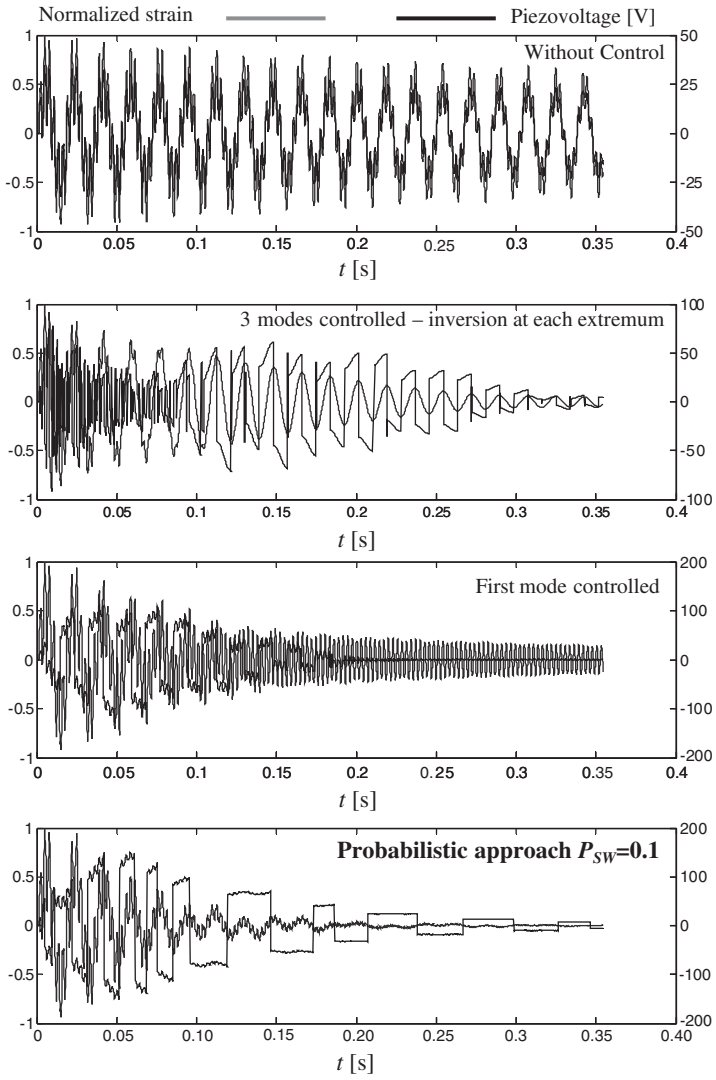


Fig. 10. Pulsed excitation—normalized strain and piezovoltage for different control laws.

selection law. Fig. 10 shows the normalized strain in the piezoelements and the piezovoltage versus time for different representative control laws. Fig. 11 shows the corresponding displacement of the beam free end. Main results in dB are summarized in Table 8.

The spectrum of the beam free end speed is plotted on Fig. 12. This figure illustrates the broadband damping capability of the proposed approach. The probabilistic control law induces simultaneously 13.0, 9.3 and 3.4 dB speed reductions for the three considered modes, on a frequency band lying between 0 and 1200 Hz. Moreover, it illustrates that the major damping is obtained for the most energetic mode, which is the first one in the considered case. More precisely, the damping performance is directly related to the energy converted on a given mode, which is an increasing function of both the mechanical energy and the coupling coefficient associated to this mode. This interesting feature is the main reason for the adaptability of the proposed process.

Inversely, the control law by mode selection cannot present this character, since, at first the controlled modes have to be selected naturally, and secondly, if all modes are selected, the process is performing best for the third mode since the switching occurs at each extremum. Moreover, if only the first mode is selected, no damping is achieved for the second and the third modes.

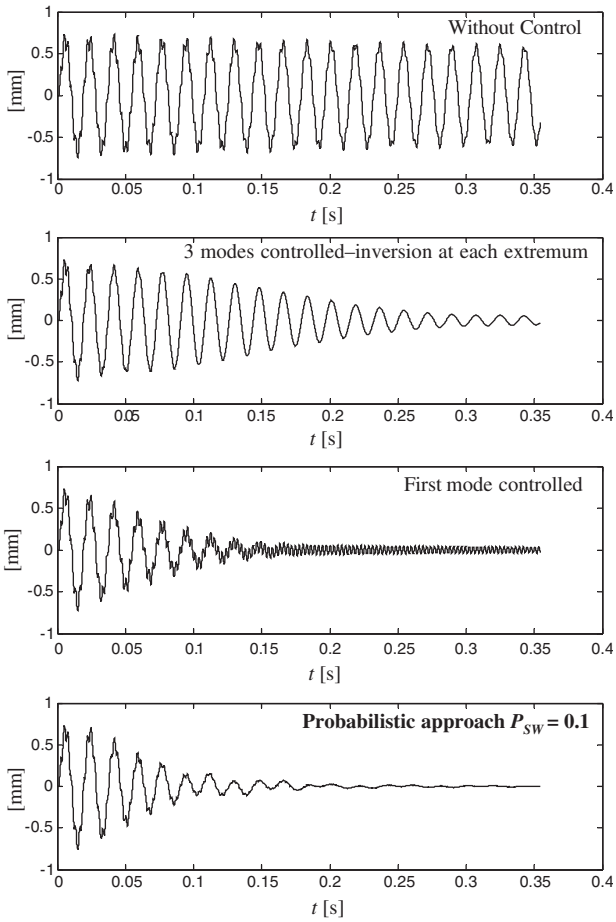


Fig. 11. Pulsed excitation—displacement of the beam free end for different control laws.

Table 8
Simulation results for a pulsed excitation

| Control Law | $A_{E\mathrm{dB}}$ | $A_{u\mathrm{dB}}$ |
|---|---|---|
| *Modes selection* | | |
| 000—without control | 0 | 0 |
| 100 | −3.45 | **−7.62** |
| 010 | −1.43 | −0.0461 |
| 001 | −0.311 | 0.0145 |
| 110 | **−5.41** | −5.06 |
| 101 | −2.56 | −3.78 |
| 011 | −1.61 | −0.0700 |
| 111—switch on each extremum | −4.89 | −3.81 |
| Probabilistic—$P_{\mathrm{SW}} = 0.1$ | **−6.50** | **−7.67** |

Bold numbers correspond to the highest damping for each technique (modes selection or probabilistic approach).

### 4.4. Simulations for a white-noise excitation

In this section, a white-noise excitation is applied at the free end of the beam. The same simulations are achieved as in the previous section. Calculations are performed for 200 periods of the first resonance frequency, with the same time steps as previously.

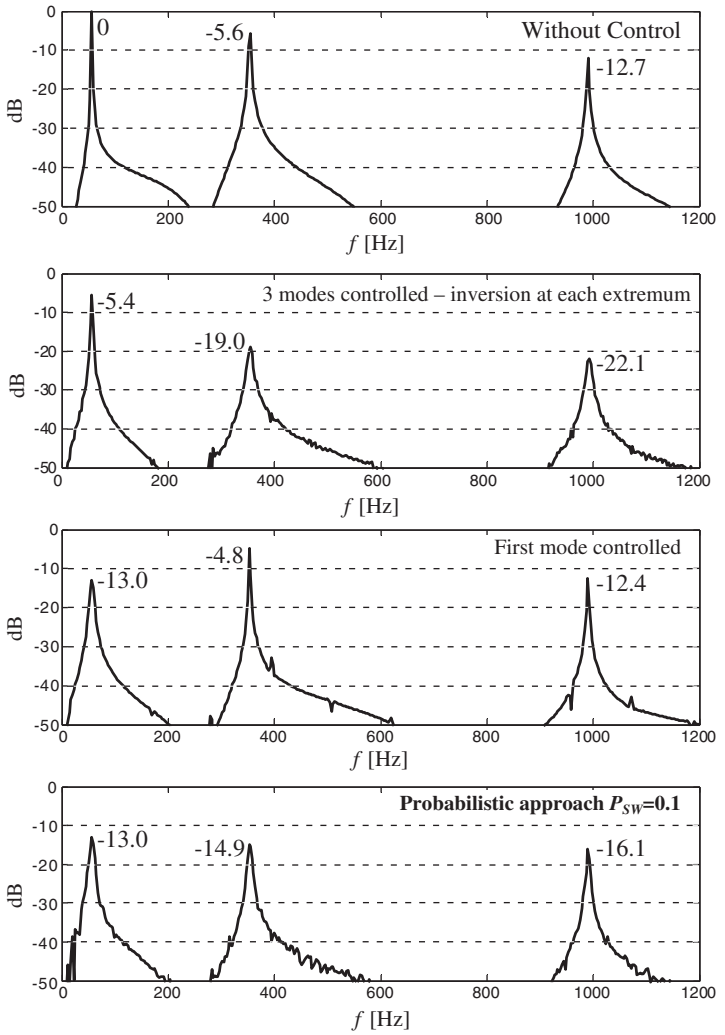


Fig. 12. Pulsed excitation—spectrum of the speed of the beam free end for different control laws.

Figs. 13–16 show the same results as in the previous section. Using the probabilistic approach, it is shown in Fig. 13 that the displacement and energy damping are optimized for almost the same value of $P_{SW}$. The optimized displacement and energy damping are $-8.5$ and $-6.3$ dB whereas it is $-3.0$ and $-4.3$ dB, respectively, when switching on all strain extrema.

Fig. 14 shows a comparison of both modes selection law and probabilistic law when $P_{SW} = 0.1$. When using the modes selection law, it is shown that the best energy damping is obtained when controlling the first and the second modes. It reaches then $-5.1$ dB which is not as good as the $-6.3$ dB obtained with the probabilistic approach. When considering the displacement, the best damping is obtained when controlling only the first mode. It reaches then $-8.8$ dB which is slightly better than the $-8.5$ dB obtained with the probabilistic approach. As in the previous section, these simulations show that the probabilistic approach allows to simultaneously optimize both energy and displacement damping.

The normalized strain and the piezovoltage as well as the displacement of the beam free end are plotted in Figs. 15 and 16, respectively. These figures are plotted for different representative control laws. Only a small part of the whole simulated time is represented on these plots. Main results in dB are summarized in Table 9.

The spectrum of the beam free end speed is plotted on Fig. 17, for different control law, in the case of a white-noise excitation. Qualitatively, the performance comparison is the same as in the pulse

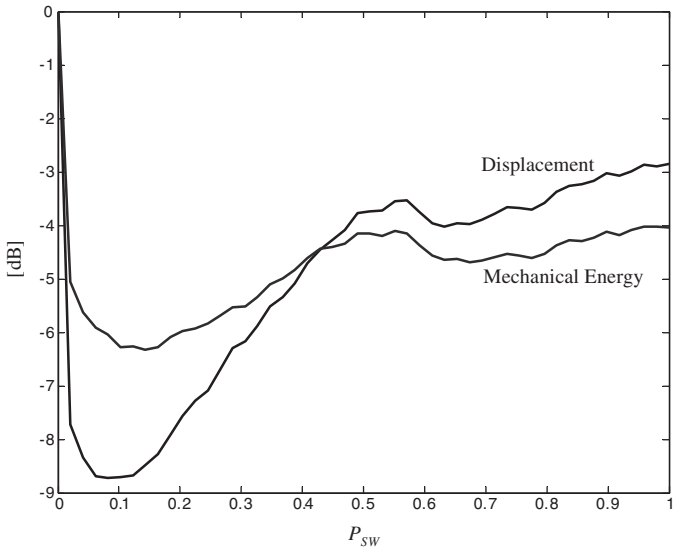


Fig. 13. White-noise excitation—displacement and energy damping with the probabilistic law as a function of $P_{SW}$.

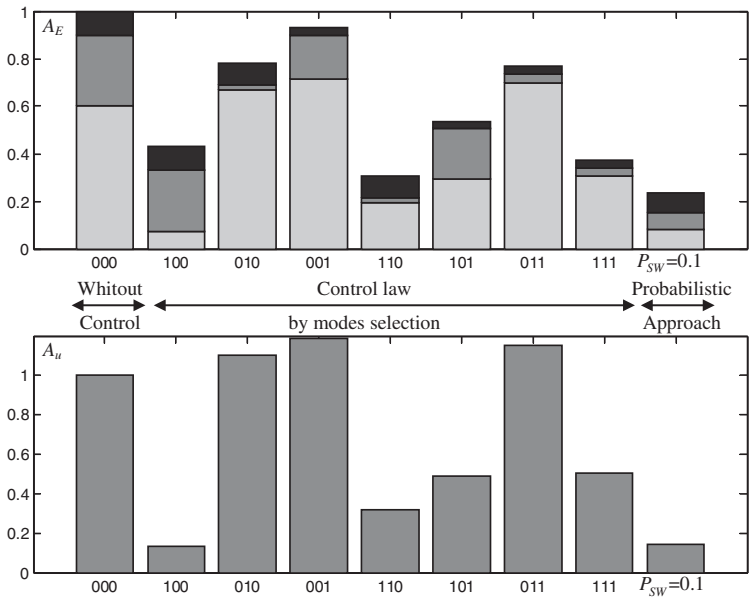


Fig. 14. White-noise excitation—energy and displacement damping with both modes selection law and probabilistic law.

excitation case. Since the proposed probabilistic control law mainly addresses the highest resonance peaks of the spectrum (weight by the corresponding coupling coefficient), the process leads to a levelled down spectrum.

## 5. Conclusion

The novel multimodal probabilistic approach described in this paper is dedicated to the SSD technique. It was shown that this control law allows to simultaneously optimize both displacement-based and energy-based

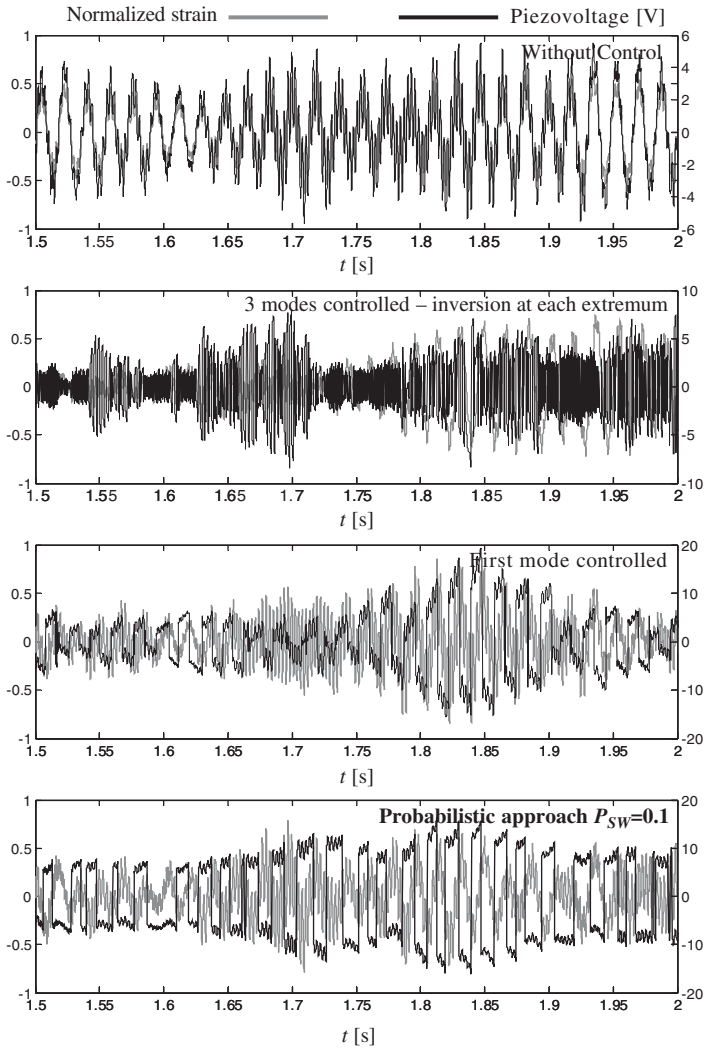


Fig. 15. White-noise excitation—normalized strain and piezovoltage for different control laws.

vibration control criteria. It is much more effective than the original control law consisting processing the piezovoltage on each strain extrema. Moreover, it is at least as efficient as the control law by modes selection which cannot optimize simultaneously both displacement and energy damping. It can also be noted that results obtained using the control law by modes selection are very likely overestimated; since simulations have been done considering that the modes could be separated without inducing any time shift. Practically, filtering devices have to be used. This necessarily induces time delay between the strain and the filtered voltage time waveforms resulting in a lack of effectiveness of the switching sequence and a drop of the damping performances. The probabilistic control law is also very easy to implement, since it does not require any filtering device or any information related to the modes of the structure. Consequently, the proposed approach is not sensitive to the boundary conditions or to any resonance frequencies drifts. The only required information is the piezovoltage itself and the strain in the piezoelements which can be obtained from an additional piezoelement used as sensor or from the processed voltage itself. Current work consists in implementing this technique on a digital signal processor (DSP) and testing it on a real experimental set-up.

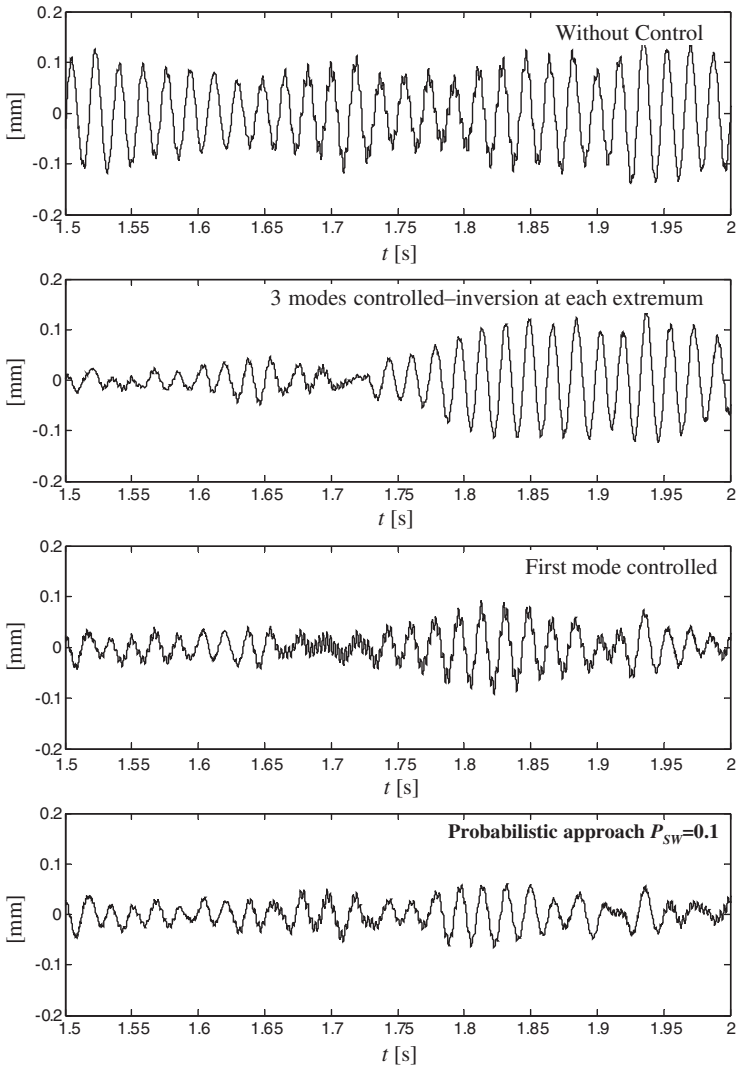


Fig. 16. White-noise excitation—displacement of the beam free end for different control laws.

Table 9
Simulation results for a white-noise excitation

| Control law | $A_{E\mathrm{dB}}$ | $A_{u\mathrm{dB}}$ |
|---|---|---|
| *Modes selection* | | |
| 000—without control | 0 | 0 |
| 100 | −3.64 | **−8.79** |
| 010 | −1.08 | 0.42 |
| 001 | −0.31 | 0.74 |
| 110 | **−5.11** | −4.96 |
| 101 | −2.70 | −3.08 |
| 011 | −1.14 | 0.62 |
| 111—switch on each extremum | −4.27 | −2.96 |
| Probabilistic—$P_{\mathrm{SW}} = 0.1$ | **−6.32** | **−8.49** |

Bold numbers correspond to the highest damping for each technique (modes selection or probabilistic approach).

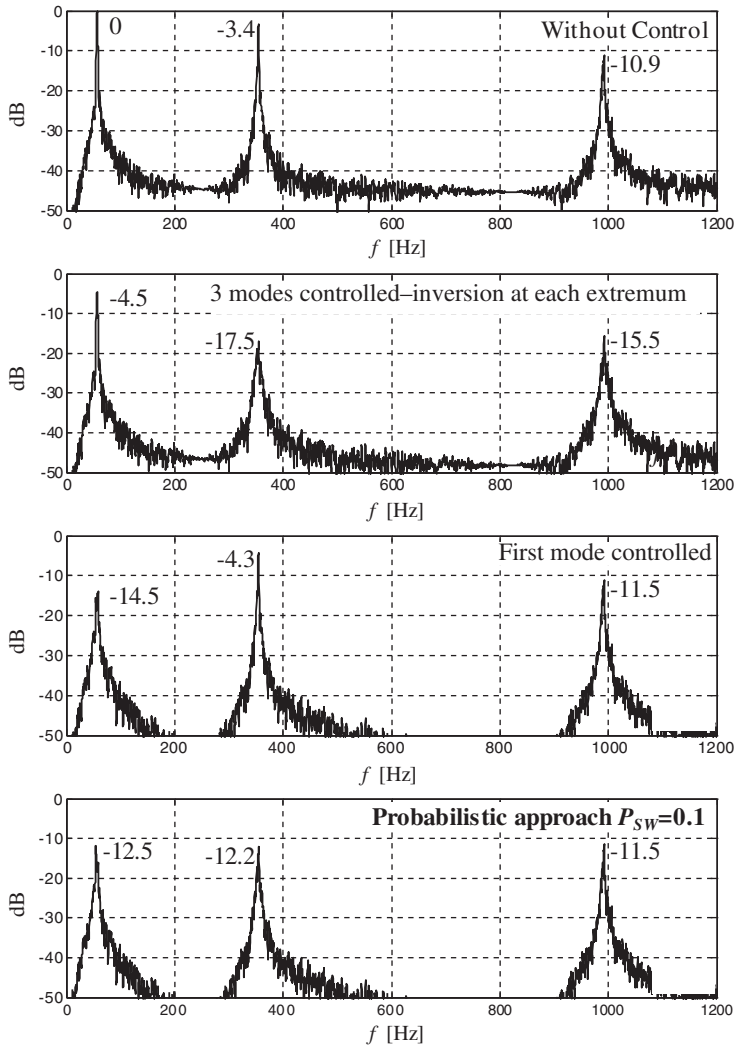


Fig. 17. White-noise excitation—spectrum of the speed of the beam free end for different control laws.

## References

[1] N.W. Hagood, A. Von Flotow, Damping of structural vibrations with piezoelectric material and passive electrical networks, *Journal of Sound and Vibration* 146 (1991) 243.

[2] S. Wu, Method for multiple shunt damping of structural vibration using a single PZT transducer, in: *Proceedings of the SPIE International Symposium on Smart Structures and Materials. Conference*, *Passive Damping and Isolation*, San Diego, Vol. 3327, 1998, p. 159.

[3] C.L. Davis, G.A. Lesieutre, An actively tuned solid-state vibration absorber using capacitive shunting of piezoelectric stiffness, *Journal of Sound and Vibration* 232 (2000) 601–617.

[4] R.A. Morgan, K.W. Wang, Active-passive piezoelectric absorbers for systems under multiple non-stationary harmonic excitations, *Journal of Sound and Vibration* 255 (4) (2002) 685–700.

[5] W.W. Clark, Vibration control with state-switching piezoelectric material, *Journal of Intelligent Material Systems and Structures* 11 (2000) 263.

[6] G.D. Larson, P.H. Rogers, W. Munk, State switched transducers: a new approach to high-power low frequency, underwater projectors, *Journal of the Acoustical Society of America* 103 (3) (1998) 1428–1441.

[7] K.A. Cunefare, State-switched absorber for vibration control of point-excited beams, *Journal of Intelligent Material Systems and Structures* 13 (2002) 97–105.

[8] C. Richard, D. Guyomar, D. Audigier, G. Ching, Semi passive damping using continuous switching of a piezoelectric device, in: *Proceedings of the SPIE International Symposium on Smart Structures and Materials. Conference*, *Passive Damping and Isolation*, San Diego, Vol. 3672, 1998, p. 104.

[9] C. Richard, D. Guyomar D. Audigier, H. Bassaler, Enhanced semi-passive damping using continuous switching of a piezoelectric device on an inductor, in: *Proceedings of the SPIE International Symposium on Smart Structures and Materials. Conference*, *Passive Damping and Isolation*, Vol. 3989, 2000, p. 288.

[10] D. Guyomar, C. Richard, L. Petit, Non-linear system for vibration damping, in: *Proceedings of the 142th ASA Meeting*, St. Lauderdale, 2001.

[11] L.R. Corr, W.W. Clark, A novel semi-active multi-modal vibration control law for a piezoceramic actuator, *Transactions of the ASME* 125 (2003) 214–222.

[12] H.A. Sodano, G. Park, D.J. Inman, Estimation of electrical charge output for piezoelectric energy harvesting, *Strain* 40 (2004) 49–58.